The Astrophysical Journal Letters, 900:L31 (7pp), 2020 September 10 https://doi.org/10.3847/2041-8213/abb082

Carbon Isotope Ratios in Planetary Nebulae: The Unexpected Enhancement of ^{13}C

L. M. Ziurys[1,2], D. R. Schmidt[3,4], and N. J. Woolf[1]
[1] Department of Astronomy and Steward Observatory, University of Arizona, 933 N. Cherry Avenue, Tucson, AZ 85721-0065, USA
[2] Department of Chemistry and Biochemistry, University of Arizona, 933 N. Cherry Avenue, Tucson, AZ 85721-0065, USA
[3] Department of Physics and Astronomy, Swarthmore College, 500 College Avenue, Swarthmore, PA 19081-1397, USA
[4] Department of Physics and Astronomy, Franklin & Marshall College, P.O. Box 3003, Lancaster, PA 17604, USA
Received 2020 June 18; revised 2020 August 11; accepted 2020 August 15; published 2020 September 7

Abstract

The $^{12}C/^{13}C$ ratio has been measured toward a sample of planetary nebulae (PNe) using millimeter observations of CO, HCN, HNC, CN, and other species, conducted with the 12 m antenna and the Submillimeter Telescope of the Arizona Radio Observatory. The observed nebulae spanned the entire lifetime of PNe, from ∼900 to 12,000 yr, and include well-known objects such as NGC 7293 (Helix), NGC 6720 (Ring), and NGC 2440, as well as relatively unexplored nebulae (M3–28, M2–48, and M3–55). In most cases, multiple molecules and transitions were used in the ratio determination, resulting in the most accurate values available to date, with 10%–40% uncertainties. The ratios found were unexpectedly low, lying in the range $^{12}C/^{13}C$ ∼1.0 ± 0.7–13.2 ± 4.9, with an average value of 3.7—drastically less than found in the envelopes of C-rich AGB stars, and, in some cases, lower than the minimum value achieved in equilibrium CNO burning. Such low values are expected for the two O-rich nebulae studied (M2–9 and M2–48), because of insufficient third dredge-up events. However, most of the PNe observed were clearly carbon-rich, as deduced from the large number of C-bearing molecules present in them. Because nucleosynthesis ceases in the PN stage, both the C/O and the $^{12}C/^{13}C$ ratios must reflect abundances at the end of the AGB. These consistently low $^{12}C/^{13}C$ ratios, combined with the bipolar/multipolar morphologies of all planetary nebulae observed, suggest an explosive process involving proton-capture occurred at the AGB–PN transition.

Unified Astronomy Thesaurus concepts: Planetary nebulae (1249); Isotope shifts (2069); Stellar nucleosynthesis (1616); Radio astronomy (1338); Molecular spectroscopy (2095); Interstellar molecules (849)

1. Introduction

The $^{12}C/^{13}C$ ratio is a sensitive indicator of nucleosynthesis and mixing in the interior of stars (e.g., Abia et al. 2017). ^{13}C is an intermediate product of hydrogen-shell burning in the CNO cycle, important for stars with masses >1.5 $M_\odot$ on the main sequence (e.g., Wiescher et al. 2010). ^{13}C is produced in this cycle on the red giant branch (RGB), and is brought to the stellar surface by convective mixing in the first dredge-up (FDU). ^{12}C, in contrast, is created by the triple-alpha process during helium burning. He burning occurs in low- and intermediate-mass stars (∼1–10 $M_\odot$) as they ascend the asymptotic giant branch (AGB; Herwig 2005). Thermal pulsing on the AGB creates a convective envelope, which, through third dredge-up (TDU), brings the ^{12}C to the stellar surface. Note that TDU does not occur for stars of 1 $M_\odot$ and solar metallicity. Thus, low $^{12}C/^{13}C$ ratios are expected on the RGB, typically 10–25. The ratios increase on the AGB to >30, in the process creating carbon stars where C > O (e.g., Lebzelter et al. 2019). Before TDU, stars have C < O, a result of the interstellar medium being oxygen-rich (Anders & Grevesse 1989).

Observations of $^{12}C/^{13}C$ ratios in evolved stars have been conducted for decades. For example, Lambert and collaborators established $^{12}C/^{13}C$ ratios in the photospheres of carbon stars from IR spectra of C_2, CO, and CN (e.g., Smith & Lambert 1990). More recent photospheric determinations include those of Hinkle et al. (2016) and Lebzelter et al. (2019), who focused on observations of CO rovibrational bands. Extensive measurements of this ratio in the circumstellar envelopes of AGB stars have also been done in the radio regime using the isotopologues of CO, HCN, and CN (e.g., Milam et al. 2009; Ramstedt & Olofsson 2014). Overall, the results across the wavelength spectrum present a coherent picture: lower ratios for oxygen-rich stars, and higher values for carbon-rich objects. For example, in the CO survey of AGB stars by Ramstedt & Olofsson (2014), typical ratios determined for the shells with C < O were $^{12}C/^{13}C$ ∼5–15, while values of $^{12}C/^{13}C$ ∼8–46 were found for those with C > O. Milam et al. (2009) found $^{12}C/^{13}C$ ∼25–90 in C-rich AGB envelopes, based on CO and CN, and substantially lower values of $^{12}C/^{13}C$ ∼3–35 in oxygen-rich shells. Both surveys determined $^{12}C/^{13}C$ ∼2–4 for J-type stars. These peculiar C-rich objects have uncharacteristically low $^{12}C/^{13}C$ ratios, no enhancement of s-process elements, and may result from stellar mergers (e.g., Sengupta et al. 2013). Such observations also strongly suggest the presence of "extra-mixing" on the RGB and the AGB to explain the very low, or lower than expected, carbon isotopic ratios (e.g., Lederer et al. 2009; Abia et al. 2017). Here ^{12}C is fed back into the H-burning shell for further processing.

The planetary nebula (PN) phase, which follows the AGB, is the evolutionary ending for most stars. As the PN stage begins, nucleosynthesis ceases. Therefore, elemental and isotopic abundances of PNe should reflect those of the AGB/PN transition. Few studies, however, have been conducted of $^{12}C/^{13}C$ ratios in PNe (e.g., Sánchez-Contreras & Sahai 2012). An early study was carried out by Palla et al. (2000), who observed the $J = 1 \rightarrow 0$ and $2 \rightarrow 1$ transitions of ^{12}CO and ^{13}CO. These authors reported $^{12}C/^{13}C$ ratios of 9–23 in seven PNe and lower limits in others. This work was followed by measurements of the $J = 2 \rightarrow 1$ and $3 \rightarrow 2$ lines of ^{12}CO and ^{13}CO of PNe by Balser et al. (2002). Ratios of $^{12}C/^{13}C$ ∼2–31 were determined in seven sources, four from the Palla et al. sample, with lower limits in additional objects. Another study by Sánchez-Contreras & Sahai (2012) established $^{12}C/^{13}C$ ratios for proto-PNe (PPNe) and young PNe, based on the $1 \rightarrow 0$ lines

of ^{12}CO and ^{13}CO using millimeter interferometry. These authors found $^{12}C/^{13}C$ ~2–10 for O-rich objects and 10–40 for C-rich sources.

To gain further insight into stellar evolution, we have measured the $^{12}C/^{13}C$ ratio in a sample of nine PNe in multiple transitions of molecules known to be optically thin (HCN, HNC, CN, and HCO^+). The values obtained were strikingly low, $^{12}C/^{13}C$ ~1–13, with C-rich PNe composing the bulk of the sample. Furthermore, in a number of nebulae, the ratio was lower than 3.5, the minimum value achieved in equilibrium CNO burning, suggesting an explosive event at the end of the AGB. Here we present our observations, analysis, and interpretation.

2. Observations

The measurements were conducted using the Arizona Radio Observatory (ARO) from 2008 to 2019. Observations of the J (or N) = 1 → 0 transitions of ^{12}CN, ^{13}CN, H^{12}CN, H^{13}CN, HN^{12}C, H^{12}CO$^+$, and H^{13}CO$^+$ at 3 mm were performed with the ARO 12 m Atacama Large Millimeter/submillimeter Array (ALMA) prototype antenna on Kitt Peak, Arizona, or its predecessor, the former NRAO 12 m telescope. The receiver used was dual-polarization, based on ALMA Band 3 sideband-separating (SBS) mixers. The image rejection was typically greater than 15 dB, intrinsic in the mixer architecture. The temperature scale for the 12 m, T_A^*, was determined by the chopper wheel method, defined as $T_R = T_A^*/\eta_b$, where T_R is the main beam brightness temperature and η_b the main beam efficiency. Measurements taken with the original 12 m, H^{12}CO$^+$ in NGC 7293 (Helix Nebula) and H^{12}CN in M3–28, were converted to this scale from T_R^*. Backends used were combinations of the 250 kHz, 500 kHz, and 1 MHz filterbanks, operated in parallel mode for the two receiver polarizations.

Observations of the $J = 3 \rightarrow 2$ transitions of H^{12}CO$^+$, H^{13}CO$^+$, H^{12}CN, H^{13}CN, HN^{12}C, and HN^{13}C, as well as the $J = 2 \rightarrow 1$ lines of ^{12}CO and ^{13}CO, were carried out with the ARO 10 m Submillimeter Telescope (SMT) using the dual-polarization, 1.3 mm receiver, which employs ALMA Band 6 SBS mixers. The typical image rejection was ⩾14 dB, inherent in the mixers. Measurements of the $J = 3 \rightarrow 2$ transition of ^{12}CO were also performed, using a dual-polarization 0.8 mm receiver with double-sideband (DSB) mixers. The temperature scale for the SMT is T_A^*, as defined above. A 1024 channel 1 MHz filterbank was the backend.

The same instrument setup was used for isotope pairs. Data were taken in beam-switching or position-switching mode. Local oscillator shifts were performed for all measurements.

3. Results

New detections of the ^{13}C-substituted molecules in PNe are shown in Figures 1–3. Integration times are typically 5–30 hr. Spectra of the ^{12}C species are shown for comparison, some from previous studies (M2–9, M3–55, M3–28, and NGC 2440: Schmidt & Ziurys 2016, 2017a; Helix: Zack & Ziurys 2013). The line profiles between isotopologues are very similar.

Figure 1 presents spectra observed toward M2–9 (left), M3–55 (middle), and NGC 2440 (right). As shown, ^{13}CO and H^{13}CO$^+$ were detected in M2–9 (Butterfly Nebula) via their $J = 2 \rightarrow 1$ and $3 \rightarrow 2$ transitions, respectively. The $J = 3 \rightarrow 2$ transitions of both ^{12}C species are also presented. This transition was used for ^{12}CO, because the $J = 2 \rightarrow 1$ line suffers from Galactic contamination. The CO spectra appear to exhibit narrower line profiles than those of HCO^+, also an effect of Galactic contamination. This younger nebula has a complex bipolar geometry (see Schmidt & Ziurys 2016). For M3–55, lines of H^{13}CN and HN^{13}C are presented with their ^{12}C counterparts, all observed in their $J = 3 \rightarrow 2$ transitions. M3–55 is a small (~10″), middle-aged bipolar nebula that appears to be C-rich. For NGC 2440, both ^{13}CO ($J = 2 \rightarrow 1$) and H^{13}CN ($J = 3 \rightarrow 2$) transitions were detected. All observed lines, including the ^{12}C isotopologues, exhibit a double-peaked profile, as might be expected from this extended (~38″) multipolar nebula.

Figure 2 displays spectra for M3–28 and NGC 7293 (Helix). For M3–28 (left panel), the $J = 3 \rightarrow 2$ lines of H^{12}CN and H^{13}CN are presented. This older, quadrupolar nebula has an angular size of ~17″ (Tylenda et al. 2003). For the Helix (right panel), the $J = 1 \rightarrow 0$ transitions of H^{12}CO$^+$ and H^{13}CO$^+$ are displayed, measured at the (+390″, −30″) position. The position observed toward this very extended (~15′), old bipolar nebula is on the eastern edge (Zeigler et al. 2013). The orientation of the bipolar flow in the Helix is almost along the line of sight, complicating the observed line profiles; those of HCO^+ may consist of two blended velocity components.

In Figure 3, the 1 → 0 lines of H^{12}CN (left) and ^{12}CN (right) in both carbon isotopologues are shown for NGC 6720 (Ring Nebula). The ^{12}CN and ^{13}CN hyperfine structures (in red) are displayed underneath the spectra. H^{12}CN and ^{12}CN had been observed previously in the Ring by Bachiller et al. (1997); here we present new observations. The Ring Nebula extends ~1.′5; the nebula is believed to have a face-on, bipolar geometry, similar to the Helix (Edwards et al. 2014).

Table 1 lists the molecular transitions detected in the PNe and their respective intensities T_A^*, line widths, and LSR velocities, determined from Gaussian fits to the line profiles. For CN, individual hyperfine components were fitted, while the data for NGC 2440 were analyzed with a two-component, redshifted and blueshifted model. The ^{12}C isotopic line parameters, shown for clarity, were determined previously (Zack & Ziurys 2013; Schmidt & Ziurys 2016, 2017a). For K4–47, NGC 6537, and M2–48, the data came from Schmidt et al. (2018a), Schmidt & Ziurys (2019), and Edwards & Ziurys (2013, 2014).

4. Analysis

4.1. Column Density and Ratio Calculations

Molecular column densities were determined using the non-LTE radiative transfer code, RADEX (van der Tak et al. 2007). Line intensities were modeled by varying the gas kinetic temperature T_K, H_2 density, and column density for a given molecule. However, while only one to two transitions were typically detected for a given species, H_2 density and T_K have been established from previous studies of molecules with similar dipole moments (e.g., Schmidt & Ziurys 2016). For sources with two observed transitions, T_K was held constant to previously established values; where only one transition was available, the H_2 density was also fixed. The molecular data files were either taken or created from LAMDA (Schöier et al. 2005), CDMS, or BASECOL (Dubernet et al. 2013). The best fit was identified using a χ^2 analysis.

For all nebulae aside from the Helix, column densities were corrected for beam dilution, based on the optical image, as well

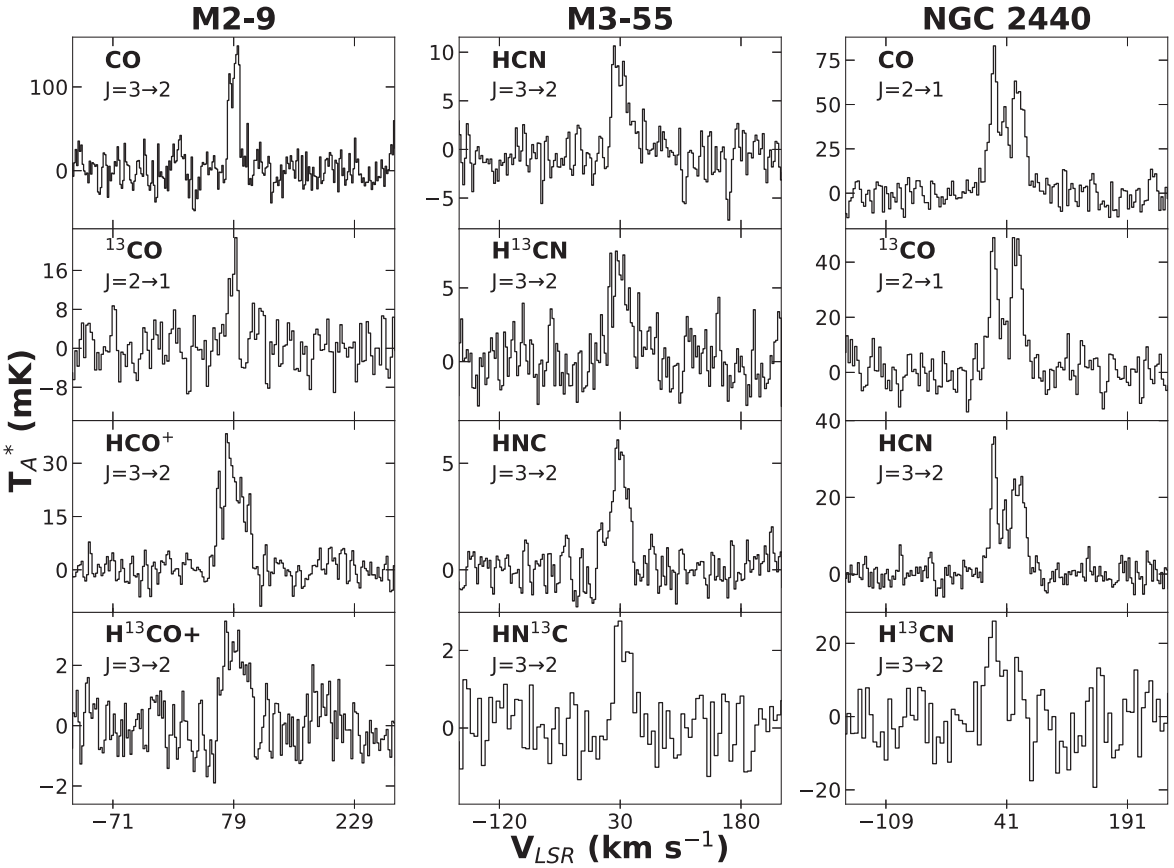

Figure 1. Spectra of the $J = 3 \rightarrow 2$ transitions of ^{12}CO, H^{12}CO$^+$, and H^{13}CO$^+$ and $J = 2 \rightarrow 1$ line of ^{13}CO, observed toward M2–9 (left); the $J = 3 \rightarrow 2$ transition of H^{12}CN, HN^{12}C, H^{13}CN, and HN^{13}C detected toward M3–55 (middle); and the $J = 2 \rightarrow 1$ lines of ^{12}CO and^{13}CO and $J = 3 \rightarrow 2$ lines of H^{12}CN and H^{13}CN, measured toward NGC 2440 (right). All data were obtained with the ARO SMT at 1 mm or 0.8 mm, with a spectral resolution of 2 MHz or 4 MHz (HN^{13}C and NGC 2440 H^{13}CN lines). Line profiles for NGC 2440 consist of redshifted and blueshifted velocity components. In M2–9, CO spectra appear to exhibit narrower profiles than HCO$^+$, a likely result of Galactic contamination.

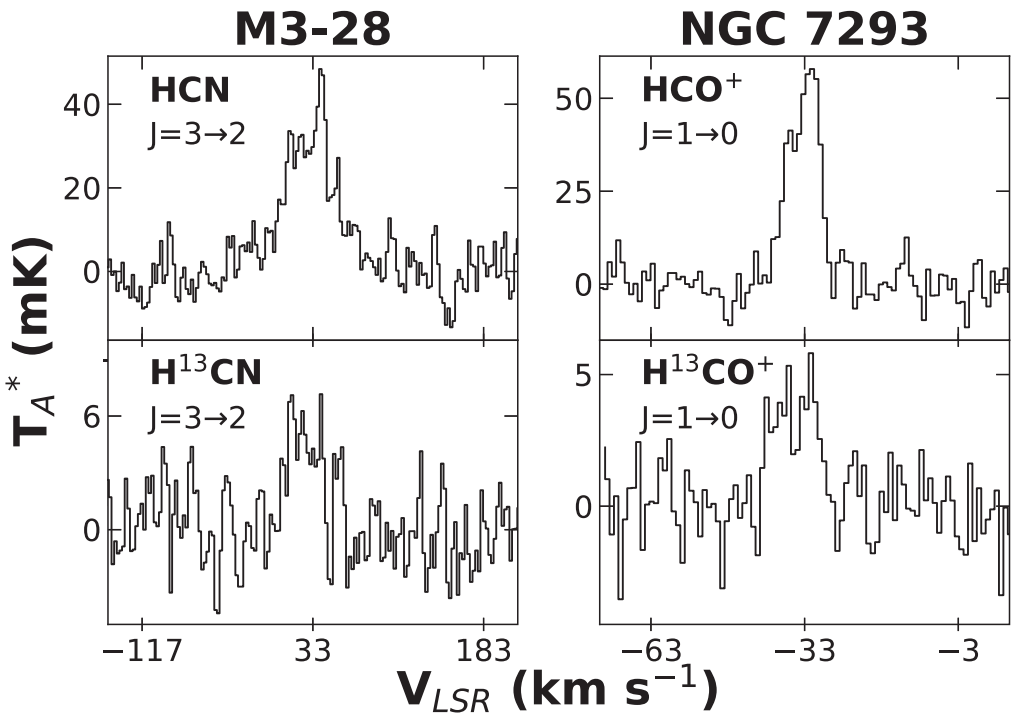

Figure 2. Spectra of the $J = 3 \rightarrow 2$ lines of H^{12}CN and H^{13}CN observed toward M3–28, observed with the ARO SMT at 1 mm (left); and the $J = 1 \rightarrow 0$ transition of H^{12}CO$^+$ and H^{13}CO$^+$, measured toward NGC 7293 (Helix Nebula) at the (+390″, −30″) position using the ARO 12 m at 3 mm (right). Spectral resolution is 2 MHz and 250 kHz for the two sources, respectively. The HCO$^+$ lines may also consist of two partially blended velocity components.

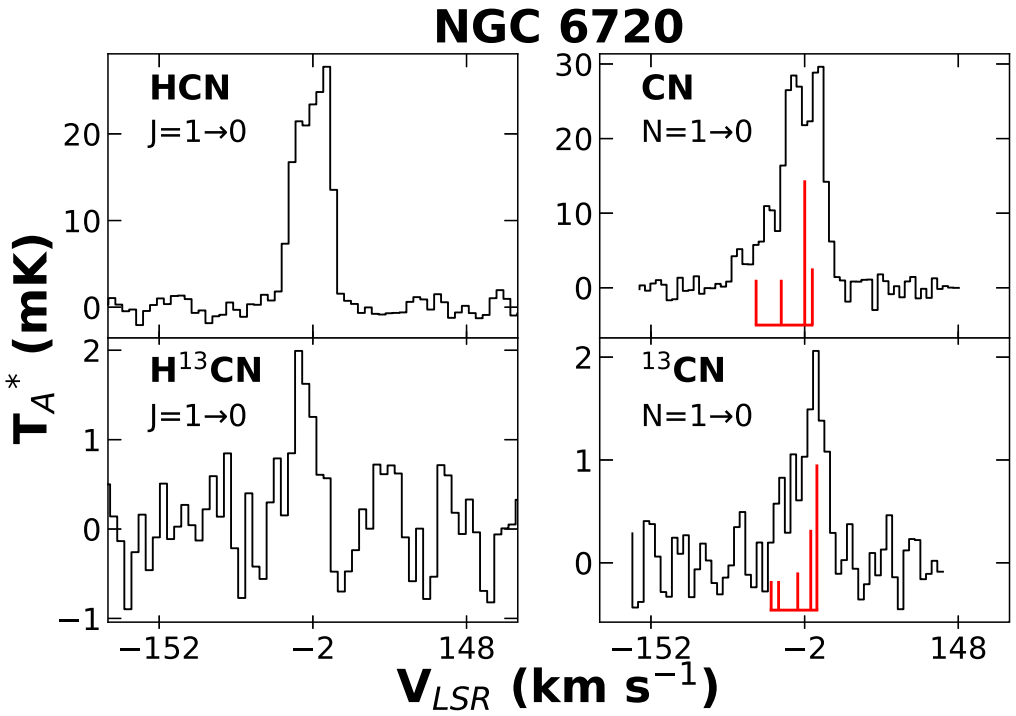

Figure 3. Spectra of the 1 → 0 transitions of $H^{12}CN$ and $H^{13}CN$ (left) and ^{12}CN and ^{13}CN (right) for NGC 6720, the Ring Nebula, observed with the ARO 12 m at 3 mm. Spectral resolution is 2 MHz. The CN hyperfine structures are displayed underneath the spectra, in red.

as a clump filling factor (see Schmidt & Ziurys 2016). Large-scale mapping of $H^{12}CO^+$ in the Helix Nebula by Zeigler et al. (2013) demonstrated that molecular and optical emission are coincident. Molecular material in PNe is also known to exist in dense clumps, as seen in H_2 (e.g., Meixner et al. 2005). The column densities are listed in Table 1.

The $^{12}C/^{13}C$ ratios (Table 2) were obtained by comparing the column densities, and are relatively insensitive to model parameters. Ratios are also listed for K4–47, NGC 6537, and M2–48. Ten species were used to determine the $^{12}C/^{13}C$ ratio in K4–47: CO, CN, HCN, HNC, HCO^+, CCH, H_2CO, HC_3N, CH_3CN, and CH_3CCH (Schmidt & Ziurys 2019). Edwards & Ziurys (2013, 2014) had obtained the spectra of both ^{12}C and ^{13}C isotopologues for NGC 6537 (HNC, HCN) and M2–48 (HCN, HNC, HCO^+, CN).

4.2. $^{12}C/^{13}C$ Ratios in Individual Sources

M3–55: This PN has the lowest ratios of 1.0 ± 0.7 and 1.8 ± 0.9, derived from HCN and HNC independently. Two transitions were observed for $HN^{12}C$, but Galactic contamination prevented measurement of the $J = 1 \rightarrow 0$ line of $H^{12}CN$ (Schmidt & Ziurys 2016).

NGC 2440: The ratios in this older PN are very low, with $^{12}C/^{13}C$ ~1.3–1.6 ± 0.5 (from CO) and 1.2–1.4 ± 0.7–1.0 (HCN), accounting for both velocity components, in good agreement. The radiative transfer analysis indicates a low opacity in the ^{12}CO $J = 2 \rightarrow 1$ line of ~0.03.

M3–28: From HCN, $^{12}C/^{13}C = 7.2 \pm 4.4$ was calculated for this older PN. Two transitions of $H^{12}CN$ were observed for this determination, but only one for $H^{13}CN$.

M2–9: The ratios in this nebula, based on HCO^+ and CO, are 13.2 ± 4.9 and 3.3 ± 1.9, respectively. There may be some Galactic contamination in CO, as mentioned, making the ratio from HCO^+ more reliable. Palla et al. (2000) reported a lower limit of >2, based on CO.

NGC 7293 (Helix): A ratio of 12.4 ± 5.4, based on HCO^+, was determined at one position (+390″, −30″) in this very large PN. In this case two lines of $H^{12}CO^+$ were observed, and one for $H^{13}CO^+$. Previous ratios measured from CO at other positions are ~9, 9.4 ± 0.6, and ~10 (Palla et al. 2000; Balser et al. 2002; Andriantsaralaza et al. 2020).

NGC 6720 (Ring): In this PN, the ratios established from HCN and CN are in good agreement with 12.2 ± 3.0 and 10.8 ± 6.3, respectively, based on the 1 → 0 transitions. From CO, Palla et al. (2000) quoted a ratio of 22 and Balser et al. (2002) found 9.5 ± 1.6.

K4–47: Derived from 10 different molecules, the ratios in K4–47 are in remarkable agreement with $^{12}C/^{13}C \approx 1.3 \pm 0.6$ to 3.4 ± 0.8. Almost all ratios were based on at least two transitions in the main isotopologue, and in many cases, in the ^{13}C species as well (Schmidt & Ziurys 2019). The lowest ratio was derived from HNC, and the highest from CO.

M2–48: Four molecules were used for the ratio determination (HCN, HNC, HCO^+, and CN), measured by Edwards & Ziurys (2014), which produced values in the range 2–4 ± 0.6. Two transitions were observed in each of $H^{12}CN$, $H^{13}CN$, $HN^{12}C$, and $HN^{13}C$, and one transition for the other two species in both isotopologues.

NGC 6537 (Red Spider): In this PN, very low ratios of 2.4 ± 0.3 and 3.5 ± 0.6 were established from HCN and HNC (Edwards & Ziurys 2013). The $J = 3 \rightarrow 2$ and 1 → 0 lines were detected in all four isotopic species.

5. Discussion

5.1. Anomalously Low $^{12}C/^{13}C$ Ratios in PNe

The $^{12}C/^{13}C$ ratios measured in the sample of nine PNe fall in the range 1.0 ± 0.7–13.2 ± 4.9, with average uncertainties <40%. In seven out of nine sources, more than one molecule was used in the determination, and often with multiple

Table 1
Molecular Observations of PNe[a]

Source	Species	Transition	T_A^* (mK)	V_{LSR} (km s^{-1})	$\Delta V_{1/2}$ (km s^{-1})	N_{tot} (cm^{-2})
M2–9	^{12}CO	$J = 3 \rightarrow 2$	140 ± 60	81.3 ± 2.7	13.6 ± 2.7	$1.0(0.5) \times 10^{16}$
	^{13}CO	$J = 2 \rightarrow 1$	22.0 ± 6.8	79.0 ± 1.4	13.0 ± 2.1	$3.0(1.0) \times 10^{15}$
	H^{12}CO$^+$	$J = 3 \rightarrow 2$	37.0 ± 3.6	80.9 ± 1.1	27.0 ± 3.3	$9.4(1.5) \times 10^{12}$
	H^{13}CO$^+$	$J = 3 \rightarrow 2$	3.0 ± 1.0	80.0 ± 1.2	25.0 ± 1.8	$7.1(2.4) \times 10^{11}$
M3–55	H^{12}CN	$J = 3 \rightarrow 2$	9.0 ± 5.0	30.1 ± 2.2	20.9 ± 2.2	$5.3(3.0) \times 10^{13}$
	H^{13}CN	$J = 3 \rightarrow 2$	8.5 ± 3.0	31.5 ± 1.8	23.0 ± 3.6	$5.3(2.0) \times 10^{13}$
	HN^{12}C	$J = 1 \rightarrow 0$	2.7 ± 0.4	29.2 ± 3.3	20.3 ± 3.3	$2.3(0.5) \times 10^{13}$
		$J = 3 \rightarrow 2$	5.6 ± 1.0	30.3 ± 2.2	23.1 ± 2.2	
	HN^{13}C	$J = 3 \rightarrow 2$[b]	3.5 ± 1.3	34.0 ± 2.7	21.0 ± 4.6	$1.3(0.6) \times 10^{13}$
M3–28	H^{12}CN	$J = 1 \rightarrow 0$	11.3 ± 5.3	∼32	∼40	$9.3(3.8) \times 10^{13}$
		$J = 3 \rightarrow 2$	33.0 ± 13.0	33.2 ± 2.2	42.2 ± 4.4	
	H^{13}CN	$J = 3 \rightarrow 2$	6.0 ± 2.8	32.0 ± 3.0	35.0 ± 4.8	$1.3(0.6) \times 10^{13}$
NGC 2440	^{12}CO	$J = 2 \rightarrow 1$[c]	80.0 ± 9.1	26.0 ± 2.0	18.0 ± 2.0	$5.1(0.8) \times 10^{15}$
		$J = 2 \rightarrow 1$[d]	70.0 ± 9.1	56.0 ± 2.0	18.0 ± 3.9	$4.5(1.1) \times 10^{15}$
	^{13}CO	$J = 2 \rightarrow 1$[c]	50.0 ± 8.4	26.0 ± 2.1	16.0 ± 3.5	$3.2(0.9) \times 10^{15}$
		$J = 2 \rightarrow 1$[d]	47.0 ± 8.4	54.0 ± 2.1	18.0 ± 3.5	$3.4(3.9) \times 10^{15}$
	H^{12}CN	$J = 1 \rightarrow 0$[c]	7.0 ± 2.0	30.0 ± 3.4	22.0 ± 3.4	$5.4(1.8) \times 10^{12}$
		$J = 1 \rightarrow 0$[d]	4.5 ± 2.0	57.0 ± 3.4	20.0 ± 5.1	$3.4(1.7) \times 10^{12}$
		$J = 3 \rightarrow 2$[c]	36.0 ± 5.0	26.0 ± 1.1	18.0 ± 2.2	
		$J = 3 \rightarrow 2$[d]	24.0 ± 5.0	56.0 ± 1.7	18.0 ± 3.9	
	H^{13}CN	$J = 3 \rightarrow 2$[c]	33.0 ± 10.0	26.0 ± 2.9	18.0 ± 5.8	$4.4(1.9) \times 10^{12}$
		$J = 3 \rightarrow 2$[d]	18.0 ± 10.0	56.0 ± 4.1	18.0 ± 3.5	$2.4(1.4) \times 10^{12}$
NGC 7293	H^{12}CO$^+$	$J = 1 \rightarrow 0$[e]	56.3 ± 7.5	−32.8 ± 1.7	8.4 ± 1.7	$4.1(0.4) \times 10^{11}$
		$J = 3 \rightarrow 2$	12.0 ± 5.0	−33.7 ± 1.1	3.3 ± 2.2	
	H^{13}CO$^+$	$J = 1 \rightarrow 0$[e]	3.7 ± 1.4	−35.7 ± 1.7	9.0 ± 1.7	$3.3(1.4) \times 10^{10}$
NGC 6720	H^{12}CN	$J = 1 \rightarrow 0$[b]	25.0 ± 1.0	−4.0 ± 3.4	38.0 ± 3.4	$7.7(0.8) \times 10^{12}$
	H^{13}CN	$J = 1 \rightarrow 0$[b]	2.0 ± 0.4	−12.0 ± 5.3	38.0 ± 3.5	$6.3(1.4) \times 10^{11}$
	^{12}CN[b]	N, J, F = 1, 3/2, 5/2 → 0, 1/2, 3/2	20.0 ± 0.9	−2.0 ± 2.7	36.0 ± 5.3	$2.7(0.4) \times 10^{13}$
		N, J, F = 1, 3/2, 3/2 → 0, 1/2, 1/2	7.4 ± 0.9	−2.0 ± 2.7	36.0 ± 5.3	
		N, J, F = 1, 3/2, 1/2 → 0, 1/2, 1/2	5.9 ± 0.9	−2.0 ± 2.7	36.0 ± 5.3	
	^{13}CN[b]	N, F_2, F = 1, 2, 3 → 0, 1, 2	1.3 ± 0.7	∼−2	28.0 ± 5.5	$2.5(1.4) \times 10^{12}$

Notes.
[a] Quoted uncertainties are 3σ; measured with 1 MHz resolution unless noted.
[b] Measured with 2 MHz resolution.
[c] Blueshifted component.
[d] Redshifted component.
[e] Measured with 250 kHz resolution.

transitions. Values are very consistent between molecules. It is therefore clear in this sample, many of which are C-rich PNe, that the $^{12}C/^{13}C$ ratios are unexpectedly low—significantly less than in normal carbon stars. Furthermore, in several nebulae, the ratio is <3.5, the minimum achieved in equilibrium CNO burning (Herwig 2005).

The objects chosen here have ages ∼900–12,000 yr (see Edwards et al. 2014; Schmidt & Ziurys 2016), and thus sample

Table 2
$^{12}C/^{13}C$ Isotope Ratios in PNe

Source	Morphology	Molecular Tracers	$^{12}C/^{13}C$	Previous $^{12}C/^{13}C$[a]	C/O	Progenitor Mass (M_{sol})
NGC 6537	Multipolar	HCN, HNC	2.4 ± 0.3 (HCN), 3.5 ± 0.6 (HNC)	···	0.95[b] ⩾ 1[c]	3–7[d]
M2–48	Bipolar	HCN, HNC, HCO^+, CN	2–4 ± 0.6[e]	···	<1[c]	···
K4–47	Bipolar	CO, CN, HCN, HNC, HCO^+, CCH, H_2CO, HC_3N, CH_3CN, CH_3CCH	1.3 ± 0.6 (HNC) – 3.4 ± 0.7 (CO)[e]	···	>1[f]	···
NGC 7293[g]	Bipolar	HCO^+	12.4 ± 5.4	9, 10, 9.4 ± 0.6	0.9–1[h,i] > 1[j]	2–6[h]
M3–55	Bipolar	HCN, HNC	1.0 ± 0.7 (HCN), 1.8 ± 0.9 (HNC)	···	⩾1[j]	···
M3–28	Quadrupolar	HCN	7.2 ± 4.4	···	⩾1[j]	···
M2–9	Bipolar	CO, HCO^+	3.3 ± 1.9 (CO), 13.2 ± 4.9 (HCO^+)	>2	<0.5[k]	∼1[l]
NGC 2440	Quadrupolar?	CO, HCN	1.3 ± 0.5, 1.4 ± 1.0[m], 1.6 ± 0.5, 1.2 ± 0.7[n]	···	0.5–1.9[o,i]	2.8-3.2[p]
NGC 6720	Bipolar	HCN, CN	12.2 ± 3.0 (HCN), 10.8 ± 6.3 (CN)	22, 9.5 ± 1.6	1.1[i]	>1[q]

Notes.
[a] From Palla et al. (2000), Balser et al. (2002), Andriantsaralaza et al. (2020); based on CO only.
[b] Pottasch et al. (2000).
[c] Edwards et al. (2014).
[d] Matsuura et al. (2005).
[e] Range from molecules listed.
[f] Schmidt et al. (2018a).
[g] (+390″, −30″) position.
[h] Henry et al. (1999, 2018).
[i] Ventura et al. (2017).
[j] Based on molecular content (see the text).
[k] Liu et al. (2001).
[l] Sánchez-Contreras et al. (2017).
[m] Redshifted.
[n] Blueshifted.
[o] Bernard-Salas et al. (2002).
[p] Miller et al. (2019), Henry et al. (2018).
[q] Edwards et al. (2014).

the entire PN lifespan. However, because nucleosynthesis ceases at the beginning of the PN stage, age should not play a role in the ratio values, unless there are chemical fractionation effects. Studies of over 20 PNe by Schmidt & Ziurys (2016, 2017a, 2017b), Zack & Ziurys (2013), Schmidt et al. (2018a), and Edwards et al. (2014) have shown that the molecular gas in PNe is warm, typically 20–50 K, such that fractionation is insignificant. Therefore, the low ratios reflect the end of the AGB.

5.2. The Role of C/O Ratio

The C/O ratio in PNe can be deduced from atomic lines (often problematic because of ionization corrections; Henry et al. 2018), or from the molecular content (Edwards & Ziurys 2014). The atomic C/O ratio has been estimated for five of the observed nebulae, but the molecular content has been determined for all objects. It is clear that M2–9 is oxygen-rich: the atomic C/O ratio is <0.5, and the nebula lacks common C-bearing molecules such as HCN. M2–48 appears to be O-rich, as well, given the presence of SO, SO_2, and SiO and the lack of CCH (Edwards & Ziurys 2014). For NGC 2440, which has abundant HCN, the situation is unclear, with C/O ∼0.5–1.9. Based on the presence of molecules such as CCH and c-C_3H_2, K4–47, M3–28, M3–55, the Ring, and the Helix are all C-rich (Schmidt & Ziurys 2017a, 2017b; Schmidt et al. 2018a, 2018b). The best estimates of the C/O ratios from atomic data are 0.9–1.0 and 1.1 for the Helix and the Ring, respectively, consistent with the molecular content; NGC 6537 has an atomic C/O ∼0.95 (see Table 2). Overall, the sample roughly reflects the C/O ratios in Galactic PNe, where ∼50% are C-rich (Ventura et al. 2017).

For the O-rich PNe, low $^{12}C/^{13}C$ ratios are perhaps expected. Oxygen-rich AGB stars typically have $^{12}C/^{13}C$ ∼5–30 (Ramstedt & Olofsson 2014), as they have not undergone sufficient TDU events to dredge up the additional ^{12}C. On the other hand, for the C-rich PNe, the ratios of 1–12 are far lower than what is found for C-rich AGB stars, which are 34–150 (Lederer et al. 2009; Milam et al. 2009; Ramstedt & Olofsson 2014). The C-rich PNe may have all originated from J-type stars, which are C-rich with $^{12}C/^{13}C$ ∼2–3 (Milam et al. 2009). J-type stars compose about 15% of the AGB population (Abia et al. 2017). Therefore, statistically, at

most two PNe in the sample might have J-type progenitor stars. Ongoing studies of the $^{14}N/^{15}N$ ratios in these PNe may give further insight into J-star origins (D. Schmidt et al. 2020, in preparation). A $^{14}N/^{15}N$ ratio of ~14 was already found in K4–47 (Schmidt et al. 2018a).

Another possibility for lowering the $^{12}C/^{13}C$ ratio is hot bottom burning (HBB). HBB is thought to occur for the higher-mass AGB stars ($M > 4\ M_{\odot}$). It arises during He-shell burning, when the bottom of the convective envelope reaches into the H-burning shell, dredging up ^{13}C and converting ^{12}C to ^{14}N. HBB can therefore transform a C-rich envelope into an O-rich one (e.g., García-Hernández et al. 2013). In the sample here, however, only two nebulae may be sufficiently massive: Helix and NGC 6537, and both have C/O ~1 (see Table 2).

5.3. Additional Processes in the Late AGB Phase

Extra, nonstandard mixing is thought to occur during both the RGB and AGB phases (e.g., Lederer et al. 2009) The very low $^{12}C/^{13}C$ ratios measured here in C-rich PNe support yet another event on the AGB. A process must occur that produces excess ^{13}C, and brings it quickly to the stellar surface before it is destroyed. Furthermore, a nonspherical expansion must be created, as all the nebulae studied here are either bipolar or multipolar. The mechanism that transforms spherical AGB shells into such structures in PNe is currently uncertain (e.g., Balick & Frank 2002).

Bedding et al. (2011) have shown that non-radial oscillations can occur in stars during helium-core burning, with the $l = 1$ "dipole mode" being common. Such dipole oscillations could occur in the He shell on the AGB and be driven to high amplitudes by a helium-shell flash, creating an explosive, predominantly bipolar expansion. This explosive flow carries helium and carbon from the He shell into the bottom of the hydrogen zone. The hot hydrogen reacts with the incoming energized carbon to produce ^{13}C through proton addition, which is subsequently ejected from the star in the explosive event. This scenario has been used to explain the extreme ^{13}C and ^{15}N enrichments in the highly collimated outflow in K4–47 (Schmidt et al. 2018a). Further detail will be given in N. Woolf et al. (2020, in preparation). Explosive production of ^{13}C through ^{12}C and ejection from the envelope was first explored by Dominy (1984).

This work was supported by NSF grant AST-1907910.

ORCID iDs

L. M. Ziurys https://orcid.org/0000-0002-1805-3886
D. R. Schmidt https://orcid.org/0000-0001-7519-6819

References

Abia, C., Hedrosa, R. P., Domínguez, I., & Straniero, O. 2017, A&A, 599, A39
Anders, E., & Grevesse, N. 1989, GeoCoA, 53, 197
Andriantsaralaza, M., Ziljstra, A., & Avison, A. 2020, MNRAS, 491, 758
Bachiller, R., Forveille, T., Huggins, P. J., & Cox, P. 1997, A&A, 324, 1123
Balick, B., & Frank, A. 2002, ARA&A, 40, 439
Balser, D. S., McMullin, J. P., & Wilson, T. L. 2002, ApJ, 572, 326
Bedding, T. R., Mosser, B., & Huber, D. 2011, Natur, 471, 608
Bernard-Salas, J., Pottasch, S. R., Feibellman, W. A., & Wesselius, P. R. 2002, A&A, 387, 301
Dominy, J. F. 1984, ApJSS, 55, 27
Dubernet, M.-L., Alexander, M. H., Ba, Y. A., et al. 2013, A&A, 553, A50
Edwards, J. L., Cox, E. G., & Ziurys, L. M. 2014, ApJ, 791, 79
Edwards, J. L., & Ziurys, L. M. 2013, ApJL, 770, L5
Edwards, J. L., & Ziurys, L. M. 2014, ApJL, 794, L27
García-Hernández, D. A., Zamora, O., Yagüe, A., et al. 2013, A&A, 555, L3
Henry, R. B. C., Kwitter, K. B., & Dufour, R. J. 1999, ApJ, 517, 782
Henry, R. B. C., Stephenson, B. G., Miller Bertolami, M. M., Kwitter, K. B., & Balick, B. 2018, MNRAS, 473, 241
Herwig, F. 2005, ARA&A, 43, 435
Hinkle, K. H., Lebzelter, T., & Straniero, O. 2016, ApJ, 825, 38
Lebzelter, T., Hinkle, K. H., Straniero, O., et al. 2019, ApJ, 886, 117
Lederer, M. T., Lebzelter, T., Cristallo, S., et al. 2009, A&A, 502, 913
Liu, X.-W., Barlow, M. J., & Cohen, M. 2001, MNRAS, 323, 343
Matsuura, M., Zijlstra, A. A., Gray, M. D., Molster, F. J., & Waters, L. B. F. M. 2005, MNRAS, 363, 628
Meixner, M., McCullough, P., Hartman, J., Son, M., & Speck, A. 2005, AJ, 130, 1784
Milam, S. N., Woolf, N. J., & Ziurys, L. M. 2009, ApJ, 690, 837
Miller, T. R., Henry, R. B. C., Balick, B., et al. 2019, MNRAS, 482, 278
Palla, F., Bachiller, R., Stanghellini, L., Tosi, M., & Galli, D. 2000, A&A, 355, 69
Pottasch, S. R., Beintema, D. A., & Feibelman, W. A. 2000, A&A, 363, 767
Ramstedt, S., & Olofsson, H. 2014, A&A, 566, A145
Sánchez-Contreras, C., Báez-Rubio, A., Alcolea, J., Bujarrabal, V., & Martín-Pintado, J. 2017, A&A, 603, A67
Sánchez-Contreras, C., & Sahai, R. 2012, ApJSS, 203, 16
Schmidt, D. R., Woolf, N. J., Zega, T. J., & Ziurys, L. M. 2018a, Natur, 564, 378
Schmidt, D. R., Zack, L. N., & Ziurys, L. M. 2018b, ApJL, 864, L31
Schmidt, D. R., & Ziurys, L. M. 2016, ApJ, 817, 175
Schmidt, D. R., & Ziurys, L. M. 2017a, ApJ, 835, 79
Schmidt, D. R., & Ziurys, L. M. 2017b, ApJ, 850, 123
Schmidt, D. R., & Ziurys, L. M. 2019, ApJL, 881, L38
Schöier, F. L., van der Tak, F. F. S., van Dishoeck, E. F., & Black, J. H. 2005, A&A, 432, 369
Sengupta, S., Izzard, R. G., & Lau, H. H. B. 2013, A&A, 559, A66
Smith, V. V., & Lambert, D. L. 1990, ApJSS, 72, 387
Tylenda, R., Siodmiak, N., Gorny, S. K., Corradi, R. L. M., & Schwarz, H. E. 2003, A&A, 405, 627
van der Tak, F. F. S., Black, J. H., Schöier, F. L., Jansen, D. J., & van Dishoeck, E. F. 2007, A&A, 468, 627
Ventura, P., Stanghellini, L., Dell'Agli, F., & García-Hernández, D. A. 2017, MNRAS, 471, 4648
Wiescher, M., Görres, J., Uberseder, E., Imbriani, G., & Pignatari, M. 2010, ARNPS, 60, 381
Zack, L. N., & Ziurys, L. M. 2013, ApJ, 765, 112
Zeigler, N. R., Zack, L. N., Woolf, N. J., & Ziurys, L. M. 2013, ApJ, 778, 16